# Commonalities in frequency-dependent viscoelastic damping in glasses in the MHz to THz regime

Cite as: J. Appl. Phys. 122, 145103 (2017); https://doi.org/10.1063/1.5006036 Submitted: 07 April 2017 . Accepted: 20 September 2017 . Published Online: 09 October 2017

Raghavan Ranganathan, Yunfeng Shi, and 🗓 Pawel Keblinski







#### ARTICLES YOU MAY BE INTERESTED IN

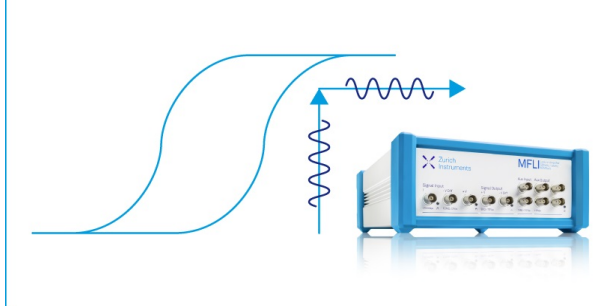
Structural vs. compositional disorder in thermal conductivity reduction of SiGe alloys Journal of Applied Physics 122, 045104 (2017); https://doi.org/10.1063/1.4994169

Viscoelastic and dynamic properties of polymer grafted nanocomposites with high glass transition temperature graft chains

Journal of Applied Physics 126, 195102 (2019); https://doi.org/10.1063/1.5119694

Perspective: Excess-entropy scaling

The Journal of Chemical Physics 149, 210901 (2018); https://doi.org/10.1063/1.5055064



Webinar How to Characterize Magnetic Materials Using Lock-in Amplifiers





Register now





## Commonalities in frequency-dependent viscoelastic damping in glasses in the MHz to THz regime

Raghavan Ranganathan, Yunfeng Shi, and Pawel Keblinski<sup>a)</sup>
Department of Materials Science and Engineering, Rensselaer Polytechnic Institute, Troy, New York 12180, IISA

(Received 7 April 2017; accepted 20 September 2017; published online 9 October 2017)

We use non-equilibrium molecular dynamics oscillatory shear simulations to study frequency-dependent viscoelastic damping spanning nearly six decades in frequency range (MHz to THz), in a wide range of model glasses including binary glasses such as Cu-Zr metallic glass (MG), Wahnström glass and amorphous silica, and unary glasses, namely, Dzugutov glass and amorphous silicon. First, for the Cu-Zr MG, we elucidate the role of quench rate, number of shear cycles, shear amplitude, and shear temperature on the damping characteristics. We observe striking commonalities in damping characteristics for all glasses studied—(i) a peak in the loss modulus in the high-frequency regime (~THz) and (ii) persistent damping in the low-frequency regime (extending down to 10 s of MHz). The high-frequency peak is seen to overlap with the range of natural vibrational frequencies for each glass, and arises from coupling between the excited harmonic vibrational modes. On the other hand, persistent damping at intermediate and low frequencies is shown to be a result of long time-scale local, irreversible deformation. *Published by AIP Publishing*. https://doi.org/10.1063/1.5006036

#### I. INTRODUCTION

The configurationally frozen liquid-like nature of glasses plays an important role for a wide range of applications. Glasses can be formed from both inorganic materials such as oxides and metallic alloys, and organic entities such as polymers. Furthermore, one can classify inorganic glasses based on their structure, into either "network glasses" such as silicabased glasses, or "non-network" glasses such as metallic glasses. Oxide glasses, most notably, based on silica have been used for a variety of applications spanning multiple millennia, primarily for decorative purposes. More recently, silica-based glasses with additions such as sodium, boron, lead, aluminum, calcium, etc. have been designed for electrical, chemical, and optical properties. On the other hand, glasses for structural applications really picked up with the discovery of metallic glass (MG) by Duwez and co-workers<sup>2</sup> and subsequent efforts in engineering processing techniques and compositional studies.3-5 Deformation mechanisms are usually influenced by the interplay of temperature and strainrates, among other factors, and have been studied extensively for glasses, in particular, for bulk metallic glasses. 6-9 A crucial aspect in this development has been the progress in the study of structure-property relations in glasses, 10-14 understanding of which has led to glasses with exceptional mechanical properties such as enhanced plasticity, 9,15,16 strength, 16,17 and fracture toughness. 18

Glasses are also candidate materials for applications in mechanical damping. In this context, damping is time-dependent (or inversely, frequency-dependent), and typically involves structural relaxations due to inherent heterogeneities in glass (often termed as anelastic relaxation). 19,20

Viscoelastic damping has its origin in atomic-level interactions and structural features within the material that result in an out-of-sync relation between stress and strain under cyclic deformation. These mechanisms are strongly dependent on the applied shear frequency (or rate). Widely different mechanisms are usually at play while contributing to damping at different frequencies<sup>25–27</sup> and have been extensively studied for polymeric systems.<sup>28</sup> While several experimental studies have focused on characterization and mechanisms of damping *via* dynamic mechanical analysis, <sup>29–31</sup> the frequency range studied cannot exceed a few 100 Hz due to experimental limitations. A mechanistic understanding of viscoelastic damping in inorganic glasses at frequency ranges extending up to THz is currently lacking, which is the focus of this work.

Structural relaxation in glasses under static conditions, is known to be greatly influenced by the deformation rate, especially at low frequencies, and over long time-scales.<sup>32</sup> Going up the frequency scale, devices such as micromechanical and nanomechanical resonators require large quality factors (low damping),<sup>33–35</sup> operate up to GHz frequencies. The upper end of the frequency spectrum (THz range) is relevant for high-frequency damping properties in phononic interconnects,<sup>38</sup> and attenuation of sound.<sup>36,37</sup> In this regime, damping is a result of coupling between harmonic vibrational modes.<sup>39–42</sup>

Anelastic relaxation could also arise due to diffusion of species such as hydrogen trapped within glass, and has been used in tuning the damping properties of hydrogen-loaded bulk metallic glasses. <sup>21–23</sup> Anelastic relaxation can be thought of as a special case of the broader time-dependent viscoelastic damping (referred to alternatively as the internal friction, denoted as  $Q^{-I}$ , the ratio of energy dissipated to stored elastic energy over a cycle of deformation). <sup>24</sup>

a)Electronic mail: keblip@rpi.edu

Experimentally, direct measurement of viscoelastic damping is performed via the dynamical mechanical analysis. <sup>43</sup> In this technique, cyclic loading in the form of an oscillatory torque is applied to probe the stress-strain response to determine the complex modulus. Forces are applied either mechanically (routinely employed for studying soft matter<sup>28</sup> and sometimes for hard materials<sup>44,45</sup>) where typical frequencies are limited to a  $\sim$ 100 s of Hz, or via electromagnetic forces<sup>46,47</sup> to attain larger frequencies ( $\sim$ 10<sup>4</sup> Hz).

At even higher frequencies approaching vibrational frequencies (in the THz range), characterizing mechanical response via direct dynamical mechanical analysis becomes experimentally unattainable. However, three common experimental techniques that can be used to study mechanical relaxation at high frequencies include (i) Inelastic X-ray Scattering (IXS), (ii) Brillouin Light Scattering (BLS) that both utilize photon-phonon scattering processes, and (iii) broadband dielectric loss spectroscopy. IXS has been used extensively to measure sound attenuation coefficients.<sup>48</sup> Using BLS, one can typically measure elastic constants including shear modulus from phonon velocities and derive the phonon damping parameter (which is proportional to the acoustic attenuation) from the full width at half maximum of the spectra. <sup>49–51</sup> However, extending this to quantify dynamic mechanical damping from these techniques is not straightforward. Dielectric spectroscopy, on the other hand can yield valuable molecular level information in non-conducting materials including a wide variety of glass forming liquids.<sup>52–54</sup> Using this technique, relaxation processes such as  $\alpha$  and  $\beta$ relaxations have been studied extensively in many glasses. 55,56 The frequency-dependent real and imaginary components of the dielectric permittivity, and consequently, the loss tangent, are obtained by relaxation of charged entities over multiple decades in the frequency range (from  $\sim 10^{-6}$  Hz, up to THz and beyond). This is achieved by using a combination of techniques (such as direct measurement of capacitance and time-domain techniques at frequencies up to kHz, frequency response analysis for MHz, and quasi-optical spectrometers for THz frequencies) to probe the broadband frequency spectrum.<sup>54</sup> Though this technique has been very useful in understanding frequency-dependent relaxation in glasses, it requires a combination of a sophisticated experimental setup, and can only be employed for non-conducting materials. Besides, mechanisms responsible for dielectric and viscoelastic losses are often different.<sup>57</sup> In this context, molecular-level simulations are extremely useful to study viscoelastic damping over a wide range of shear frequencies, particularly in the high frequency (GHz to THz) regime. Molecular dynamics deformation studies have been used extensively<sup>14</sup> to study mechanical properties including tensile<sup>58,59</sup> and compressive deformation, <sup>60</sup> indentation, <sup>61</sup> fatigue, <sup>62</sup> and plastic deformation under shear. <sup>63,64</sup>

We had previously demonstrated that oscillatory shear based molecular dynamics simulations can be used to study frequency-dependent viscoelastic damping in hard materials such as crystalline composites comprising soft and stiff crystalline phases.<sup>25</sup> We showed that a characteristic peak in frequency-dependent damping arises in the THz regime from phonon-phonon anharmonic coupling, and essentially decays

to zero (i.e., behaves elastically) as frequency is lowered. In this work, we present non-equilibrium (NE) oscillatory shear molecular dynamics simulations to study mechanisms behind frequency-dependent loss moduli (used synonymously with viscoelastic damping or mechanical damping) in various model glasses, over a wide range of frequencies (spanning nearly six decades). Compared to the crystalline case, we uncover novel damping mechanisms in glasses - at high frequencies (~THz), a characteristic peak in damping is observed. While for crystalline systems, the primary mechanism for high-frequency damping was shown to be due to anharmonic coupling between vibrational modes, 25 the primary damping mechanism in glasses is harmonic, with the oscillatory shear exciting the vibrational eigen modes corresponding to the driving frequency. At intermediate and lower frequencies ( $\sim$ 10 s of MHz), persistent damping (albeit much lower in magnitude compared to the THz range) results from long time-scale, local irreversible deformation. We emphasize here that the "low frequency" response probed in this work (~MHz) is in the context of the frequency regime studied; it is still orders of magnitude larger than the experimental capacity (few 100 s of Hz).

The organization of the paper is as follows: the oscillatory shear methodology to characterize damping and details of model structures are presented in Sec. II. In Sec. III, we present an extensive analysis of various factors that affect damping in the Cu-Zr metallic glass, as an example system. Section IV describes the commonalities in damping behavior over a wide range of frequencies, for a range of glasses. Section V contains a discussion on the mechanisms of damping, and conclusions are presented in Sec. VI.

## II. SIMULATION METHODOLOGY AND MODEL STRUCTURES

#### A. Oscillatory shear deformation

We study viscoelastic damping in model glasses by the application of non-equilibrium oscillatory shear deformation, within the framework of molecular dynamics. The methodology behind the shear simulations is presented in detail in our previous work.<sup>25</sup> In brief, we apply a sinusoidally-varying shear strain,  $\gamma_{xy} = \gamma_o \sin(2\pi f t)$  at a shear frequency, f by tilting a face of the simulation cell with a shear amplitude,  $\gamma_a$ . We ensure that  $\gamma_o$  is well below the elastic limit to remain in the linear viscoelasticity regime (see Sec. III C for further details). The corresponding virial stress component  $(\tau_{xy})$  is computed and fitted to a sinusoidal profile at the same frequency as that of the applied strain, but with a phase shift,  $\delta$ . We then determine the frequency-dependent storage (G') and loss moduli (G'') constituting the complex shear modulus,  $G^* = G\cos(\delta) + iG\sin(\delta);$  where  $G = \tau_{xy,max}/\gamma_{xy,max},$  G' $=G\cos(\delta)$ , and  $G''=G\sin(\delta)$ .

Our typical simulation protocol consists of oscillatory shear over 5 cycles under the constant volume (NVE) condition to compute the averaged loss modulus,  $G'' = G \sin(\delta)$ . The temperature at the start of shear simulation is typically fixed at about 35% of the glass transition temperature  $(T_g)$ . A consequence of the shear process is dissipation of heat that leads to an increase in temperature; in our simulations, we

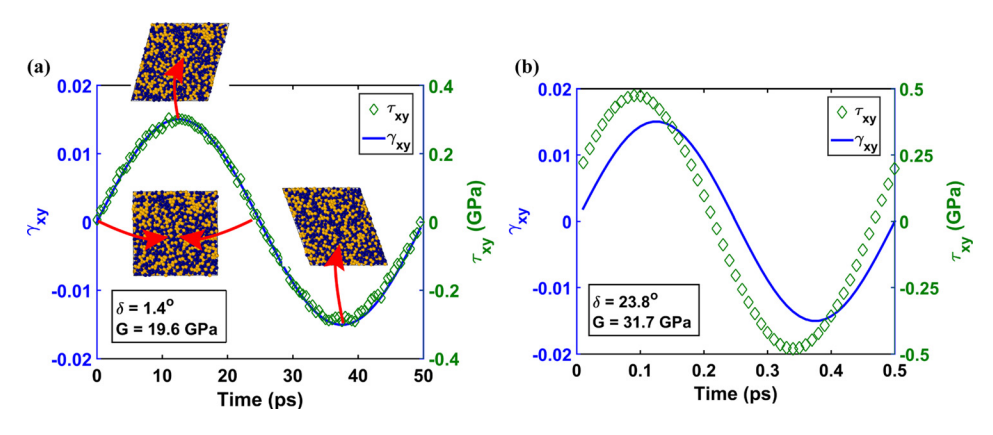


FIG. 1. Typical stress-strain response for model Cu-Zr metallic glass at (a)  $f=0.02\,\mathrm{THz}$ , exhibiting a low phase difference and low loss, and (b)  $f=2\,\mathrm{THz}$ , showing a large phase difference, and correspondingly, large loss modulus. The peak shear modulus, G is also noted. System temperature.

observe only a modest temperature rise, to the extent of a few percent for an extended range of shear frequencies. As we shall show later, in a narrow region of frequencies in the high-frequency regime (of the order of a few THz), a pronounced peak in damping is observed, that could lead to a temperature increase by  $\sim\!25\%$  in some glasses. However, we note that this is still well below the  $T_g$  and hence, possible effects on softening effects due to shear are minimal. Moduli data are also computed in the presence of a Nose–Hoover thermostat (i.e., in the NVT ensemble), over a larger number of shear cycles (300 cycles) for comparison. We also consider cases where we characterize damping for a constant amount of time as opposed to constant number of cycles, at different frequencies.

We are primarily interested in the dependence of loss modulus, (G'') on shear frequency ("frequency-sweep" simulations) and use loss modulus synonymously with damping in the rest of the paper. The shear frequency is varied over 5 decades (ranging from 10 s of MHz to 10 s of THz) where we uncover disparate mechanisms for damping at high and low frequencies. Figure 1 shows sample oscillatory shear deformation data (shear strain,  $\gamma_{xy}$  and shear stress,  $\tau_{xy}$ ) averaged over 5 cycles of shear for the Cu-Zr MG system at two shear frequencies (f=0.02 THz and f=2 THz), exhibiting markedly different  $\delta$  and G''. Temperature at the start of shear deformation was 300 K. Atomic snapshots at shear strains corresponding to zero, maximum, and minimum shear strains are shown as insets (shear strains for deformed cases are exaggerated for clarity).

#### **B.** Model structures

We study viscoelastic damping in five model glasses, namely, (a) Cu-Zr MG,<sup>67</sup> (b) Dzugutov glass,<sup>68</sup> (c) amorphous silicon (a-Si),<sup>69</sup> (d) Wahnström glass,<sup>70</sup> and (e) amorphous silica.<sup>71</sup> All the glasses have been studied extensively in literature and have been used as models for understanding structure-property relations in glasses and studying mechanical properties. 14,58,72-74 We generate the starting glass structures by quenching the melt under zero external pressure using the Nose-Hoover barostat. 75–78 For each structure, we allow at least 100 ps for equilibration at the molten state and then quench the melt with a quench rate Q. The values of Q usually attainable in computer simulations are orders of magnitude larger than in experiment and are typically in the range of 10<sup>10</sup> to 10<sup>14</sup> K/ps.<sup>67,79–82</sup> For the MG system, which forms the baseline for an extensive study on various factors affecting the damping characteristics, we additionally employ various quench rates to study the effect of quench rate on damping as described in Secs. III A and III B.

For each glass, the choice of force-field describing the interaction energy, the time-step, the quench rate, the  $T_g$ , the system size, and a few mechanical properties relevant for characterizing damping are listed in Table I.  $T_g$  was estimated from the temperature at which a change in the slope of the volume-temperature curve is observed during quench from a high temperature (liquid) to the shear temperature, at zero external pressure, and with the quench rate Q indicated. We use periodic boundary conditions along all three axes to

TABLE I. Simulation details and material properties for the five glass models used in this study.

Model/system	Cu-Zr MG	Dzugutov <sup>a</sup>	a-Si	Wahnström <sup>b</sup>	Silica
Potential	EAM <sup>67</sup>	Dzugutov <sup>68</sup>	Tersoff <sup>69</sup>	LJ <sup>70</sup>	BKS, <sup>71</sup> with Wolf summation <sup>112</sup>
					(electrostatics)
Time step (fs)	2	10.8	0.5	0.46	1.6
$T_{g}(K)$	815	418	1100	1000	2430
Quench rate $(Q, K/s)$	$8.5 \times 10^{11}$	$1.83 \times 10^{11}$	$3 \times 10^{13}$	$8.26 \times 10^{12}$	$9.8 \times 10^{12}$
Deformation temperature (K)	300	174	540	274	900
Shear modulus (G, GPa)	18.38	3.34	34.1	20.13	35.3
Elastic limit (%)	4.9	5.9	12.9	6.56	14.2
Applied strain (oscillatory shear) (%)	1.5	1.81	3.95	1.99	4.36
System size (# atoms)	16 384	27 000	27 000	32 000	24 000

<sup>&</sup>lt;sup>a</sup>For the Dzugutov glass, the fundamental length and time scale correspond to  $\sigma = 3.4 \,\text{Å}$  and  $t_o = 2.16 \,\text{ps}^{113}$  and we set the energy parameter  $\varepsilon = 0.1 \,\text{eV}$  to scale to physically relevant scales.

<sup>&</sup>lt;sup>b</sup>For the Wahnström glass, these constants correspond to  $\sigma_{22} = 2.7 \,\text{Å}$ ,  $t_o = 0.46 \,\text{ps}$ , and  $\varepsilon_{22} = 0.16 \,\text{eV}$  that correspond to a model 50–50 Ni-Nb metallic glass 61,114

simulate bulk properties. The final structures are metastable glasses characterized by pair correlation functions consistent with literature. All simulations were performed with the LAMMPS simulation package.<sup>83</sup>

#### III. DAMPING IN MG

In this section, we focus on viscoelastic damping in the equimolar Cu-Zr MG system, with an emphasis on understanding the key factors that affect damping. These include the effect of quench rate used in generating the glass, the interplay between quench rate and dependence of damping on the number of shear cycles, the effect of shear amplitude and finally, the shear temperature. For each case, we perform "frequency-sweep" oscillatory shear simulations over six decades in frequency.

#### A. Frequency-dependent loss moduli

Frequency-sweep simulations to study the frequency dependence of loss moduli (G'') were carried out for MG quenched at multiple quench rates. Figure 2 shows the variation of G'' with frequency at  $T = 300 \,\mathrm{K}$ . We observe a characteristic peak in damping in the high-frequency regime (of the order of a few THz), similar to the observation in model crystalline Lennard-Jones composites.<sup>25</sup> However, the primary mechanism for damping differs – anharmonic coupling between phonons was observed to cause damping in the THz regime for the crystalline materials, whereas, as we shall discuss later (Secs. IV A and V), the origin of this peak in glasses lies in the coupling between the harmonic vibrational modes driven by the external, non-equilibrium oscillatory shear deformation. Interestingly, we observe that the peak amplitude does not depend on the quench rate, while the intermediate and low-frequency regimes show a strong quench rate dependence. This clearly suggests that structural differences arising from differences in quench rate do not affect the highfrequency damping in the THz regime.

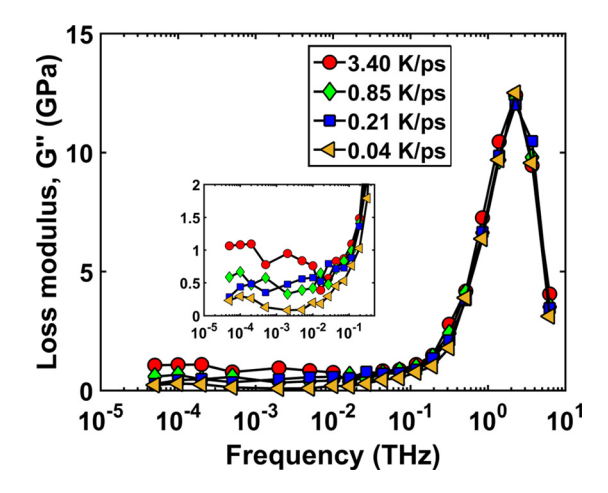


FIG. 2. Frequency-sweep simulations depicting the variation of loss modulus with shear frequency for the Cu-Zr MG system. Responses for four different quench rates are shown. The characteristic peak in the high-frequency regime overlaps for all quench rates. Low-frequency damping is affected by the quench rate, with larger quench rates resulting in larger damping. The inset shows the portion of the low-frequency regime magnified.

With decreasing frequency, damping decreases initially, following an approximate power-law scaling with frequency (see Sec. IVC for a detailed discussion), followed by nearly frequency-independent damping. However, the extent of damping in the intermediate and low frequencies (extending down to 50 MHz) shows a strong dependence on quench rate – higher quench rate exhibits larger damping (seen more clearly in inset of Fig. 2). The persistent damping in the MG system, combined with the dependence on quench rate strongly indicates that larger quench rates lead to more metastable glasses with shallower energy minima, consequences of which are greater structural relaxation and enhanced damping.

## B. Dependence of damping on the number of shear cycles

In our oscillatory shear simulations, a primary concern is the variation of calculated loss moduli with the number of shear cycles. This is particularly of interest for glasses due to their metastability. It is expected that atomic rearrangements with multiple cycles of shear could result in damping that could potentially depend on the number of shear cycles,  $N_{cycles}$ . We ideally desire a structure that does not exhibit significant cycle-dependent damping, in order to keep our simulation times tractable, especially at low frequencies. To examine this effect, we study the dependence of loss modulus on  $N_{cycles}$  for the four quench rates described in Sec. III A.

Shown in Fig. 3 are the results for damping at two frequencies,  $f = 0.5 \, \mathrm{THz}$  and  $0.5 \, \mathrm{GHz}$ , over multiple shear cycles. We perform these simulations at a constant temperature (NVT) of  $T = 300 \, \mathrm{K}$  to prevent abnormal structural rearrangements due to temperature rise. We observe that the fastest quench rate ( $Q = 3.4 \, \mathrm{K/ps}$ ), being the most metastable, results in damping that varies strongly with  $N_{cycles}$ , especially in the initial stages. For glasses quenched with  $Q = 0.85 \, \mathrm{K/ps}$  and lower, we observe fairly cycle-independent damping. We note that such cycle-independent damping is also exhibited at other frequencies and we just show two frequencies here for illustrative purposes. For all our further analyses, we use the MG sample prepared with a quenching rate Q of  $0.85 \, \mathrm{K/ps}$ .

#### C. Effect of shear amplitude

Under oscillatory shear deformation, the extent of shear amplitude determines the nature of viscoelastic response in the material. Typical viscoelastic materials exhibit a "linear" viscoelasticity up to certain amplitude, beyond which the response becomes "non-linear." The linearity in this context refers to the dynamical shear modulus (either G' or G'') being invariant with respect to the shear amplitude. This is a routine analysis in the field of dynamical shear experiments, especially in the field of soft matter such as polymer composites<sup>28</sup> where, the strain amplitude determines whether the shear falls under the so-called Small Amplitude Oscillatory Shear (SAOS) or Large Amplitude Oscillatory Shear (LAOS) regime. SAOS corresponds to a linear viscoelastic response while LAOS gives rise to non-linearity.<sup>28</sup>

In our simulations, we check for linearity in viscoelastic response by monitoring the dependence of G'' on the shear amplitude. Very low strain amplitudes result in a poor signal to

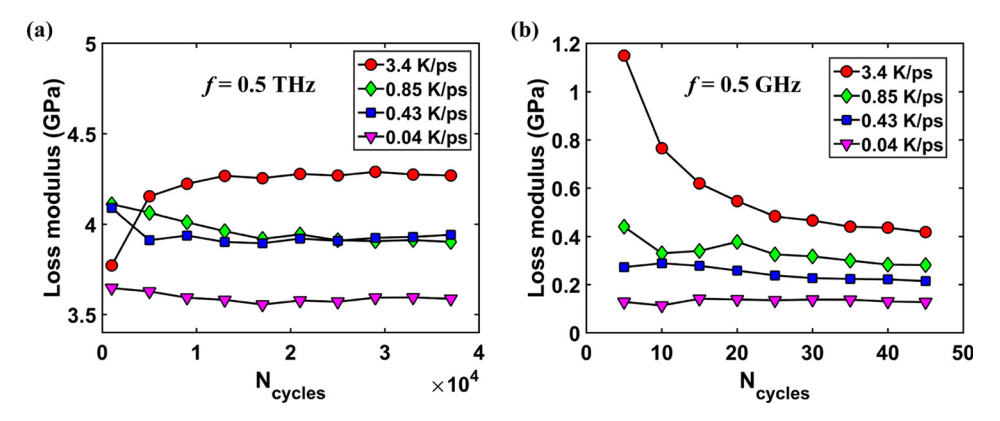


FIG. 3. Effect of aging on the computed loss modulus for glasses quenched at various rates. Aging in glass leads to estimated properties that are dependent on the number of shear cycles; this is effect is probed by varying the number of shear cycles  $(N_{cycles})$  for each quench rate. Shown in (a) and (b) are data for two widely different shear frequencies (f = 0.5 THz and f = 0.5 GHz, respectively). Simulations were performed under NVT conditions at a temperature of 300 K. The quench rate used for the bulk of the analysis pertaining to the MG, namely Q = 0.85 K/ps shows fairly cycle-independent damping.

noise ratio for the estimation of G'', especially at low frequencies. Figure 4 shows the variation of G'' with strain amplitude for four frequencies separated by an order of magnitude from each other. Simulations are performed at 300 K under NVE conditions. As seen from the figure, non-linearity in the response begins to set in at shear strains,  $\gamma_{xy} \gtrsim 0.04$ , which is also close to the elastic limit for this system (refer to Table I). We thus choose a value of  $\gamma_{xy} = 0.015$  (or 1.5%) in all our shear simulations in the MG system to ensure a good signalto-noise ratio and to simultaneously operate within the linear viscoelastic regime.

#### D. Effect of shear temperature

The predominant role played by temperature in viscoelastic response is the softening of the material, leading to more viscous character. We quantify this effect via frequency-sweep simulations at various temperatures. Figure 5 shows the variation of loss modulus with frequency for temperatures ranging from 30 K to 800 K. We note that the  $T_g$  for the glass is ~815 K. We observe that the highfrequency peak is almost invariant with respect to

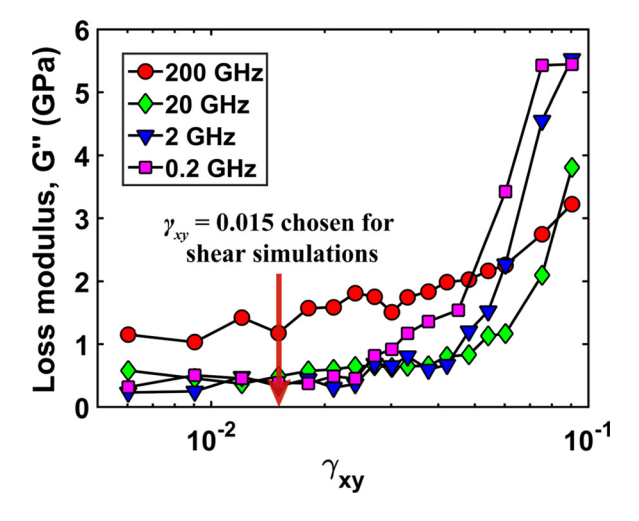


FIG. 4. Effect of shear strain amplitude on viscoelastic response in MG. Loss modulus is estimated for four different shear frequencies spanning four orders of magnitude. Significant non-linearity in the response is observed at strain amplitudes,  $\gamma_{xy}$  larger than about 0.04 (or 4%).

temperature. This is not surprising since this frequency regime corresponds to frequencies in the range of thermal vibrations, where the damping is harmonic, which is temperature invariant.<sup>39–42</sup> The softening at higher temperatures lowers the high-frequency modulus marginally.

In the lower frequency regime, however, we observe a marked difference in damping – the softening effect is sufficient to overwhelm the driving frequency and we see significant damping at higher temperatures. At 800 K (very close to the  $T_{o}$ ), we observe that at the lowest frequency ( $f = 5 \times 10^{-4}$  THz), the loss modulus begins to drop with frequency; here, although the phase shift increases marginally with lowering frequency, we observe that shear stress drops significantly (by  $\sim 60\%$ ) due to enhanced softening at this low frequency.

#### IV. COMMONALITIES IN DAMPING MECHANISMS **IN GLASSES**

#### A. Frequency-dependent damping

The frequency-dependent damping characteristics in the MG system, namely, the high-frequency peak (in the THz regime) and persistent damping in the low-frequency regime beckons the following question—"are the characteristics of

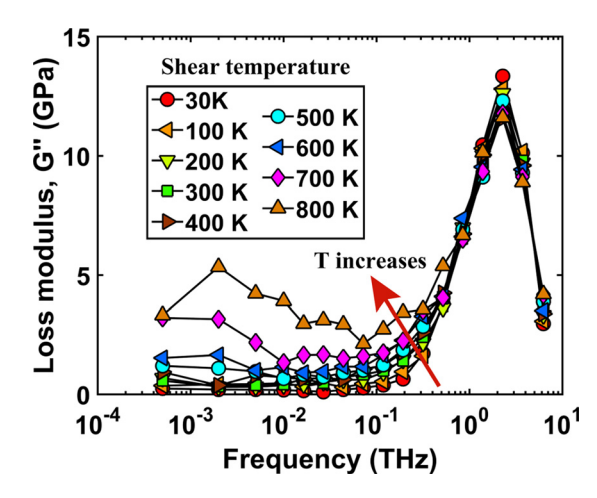


FIG. 5. Frequency-sweep simulations to study the effect of shear temperature on damping in MG. The maximum temperature (800 K) is just below the  $T_g$  for the MG, which is  $\sim 815$  K.

viscoelastic damping in glasses more universal in nature and can be understood mechanistically for a wide variety of inorganic glasses?." With this goal in mind, we extend our work to study damping in four other glasses—Dzugutov glass, amorphous silicon (a-Si), the Wahnström glass, and amorphous silica. We perform oscillatory shear deformation simulations at frequencies similar to the case of the MG system, to look for typical characteristics in the frequency-dependent damping.

Shown in Table I is the list of simulation details, the potential used for describing interactions, and various system properties considered for this work, for all the glass models. We note that we consider both unary (the Dzugutov glass and a-Si) and binary glasses (Wahnström and amorphous silica), in addition to the MG glass discussed so far, which forms the baseline for our comparison of damping characteristics. The two most important factors to be considered while comparing the damping properties between various glasses are the elastic limit and the glass transition temperature  $(T_g)$ . The former affects the linearity in viscoelastic response (as discussed in Sec. IIIC) and the latter determines the relative scaling between the temperature at which the material is deformed, and  $T_g$ , where significant softening occurs (see Sec. III D). Thus, to maintain comparative shear conditions across all glasses, we set the shear strain amplitude and the deformation temperature for the MG system as the baseline, and scale the strain amplitude and deformation temperature of the remaining four glasses based on their respective elastic limits and  $T_{\varrho}$ . The scaling is such that a common shear strain amplitude (normalized by the elastic strain limit), and a common deformation temperature (normalized by the glass transition temperature) are used for all the glasses. These values are also given in Table I.

Figure 6 shows the comprehensive damping data from frequency-sweep simulations for all the five glasses. Data plotted in red triangles correspond to data from five cycles of shear without a thermostat (i.e., under NVE conditions), and those plotted in blue triangles are from 300 cycles of shear in the high-frequency regime, in the presence of a Nose-Hoover thermostat. The latter case is to check for stationarity (i.e., invariance with respect to number of shear cycles) in the stress-strain data. We observe only negligible differences between the moduli computed for shear with and without a thermostat. Moreover, the stress-strain profiles are stationary, as observed from the Lissajous plots (shown in Fig. 7) for all five glasses at the peak damping frequency, over 300 cycles of shear. In addition, Fig. 6 also shows oscillatory shear results for a fixed amount of time (as opposed to fixed number of cycles), shown by green circle markers. Only minor differences were observed for damping for the two cases (fixed time versus fixed number of cycles). We note that the fixed time simulations (data shown by green circle markers) were run for  $\sim$ 50 ns that corresponds to 5 cycles of shear at the lowest frequency, and 5000 cycles at the highest frequency.

Striking commonalities in the damping characteristics are observed according to Fig. 6—first, in the high-frequency regime (ranging from  $\sim$ 0.1 THz to  $\sim$ 10 s of THz), all glasses show a pronounced peak in damping. With decreasing frequency starting from the peak, G'' decreases as an approximate power law (as shown later in Fig. 10) over an intermediate frequency window for all glasses. Lastly, with further reduction

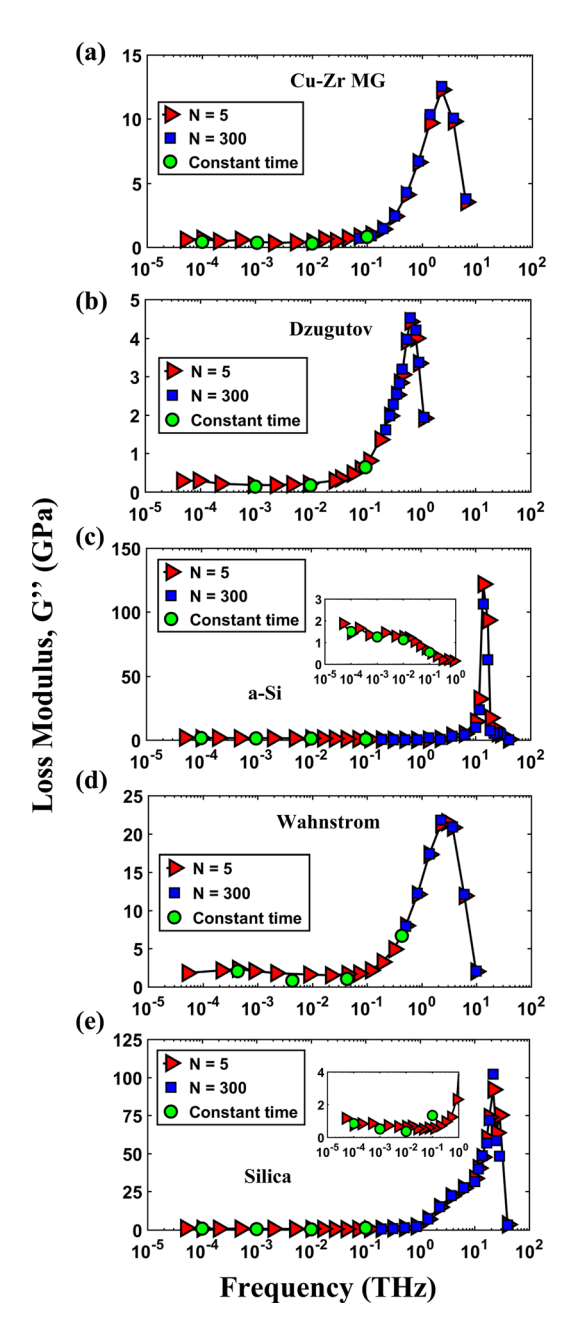


FIG. 6. Frequency-sweep simulations for the five glass structures considered in this work. For each glass, we show the variation of loss modulus as a function of shear frequency. All glasses show a characteristic peak in the high-frequency regime, and a nearly-invariant, finite damping in the low-frequency regime (insets for a-Si and silica show the magnified portion of the low-frequency regime). Data shown in red (▲) correspond to 5 cycles of shear under NVE, those in blue (■) correspond to 300 cycles under NVT, and green symbols (●) correspond to moduli computed during shear for a constant amount of time as opposed to the constant number of cycles.

in frequency, persistent (even weakly increasing in some cases) damping is observed in all glasses, extending down to the MHz regime. This is true irrespective of whether shear was performed over a fixed number of cycles, or for a fixed amount of time. The mechanisms behind these damping characteristics are discussed in the following sections (Sec. IV B–IV D).

#### B. High-frequency damping

In our previous work in damping in crystalline composites, we showed that enhanced damping at frequencies in

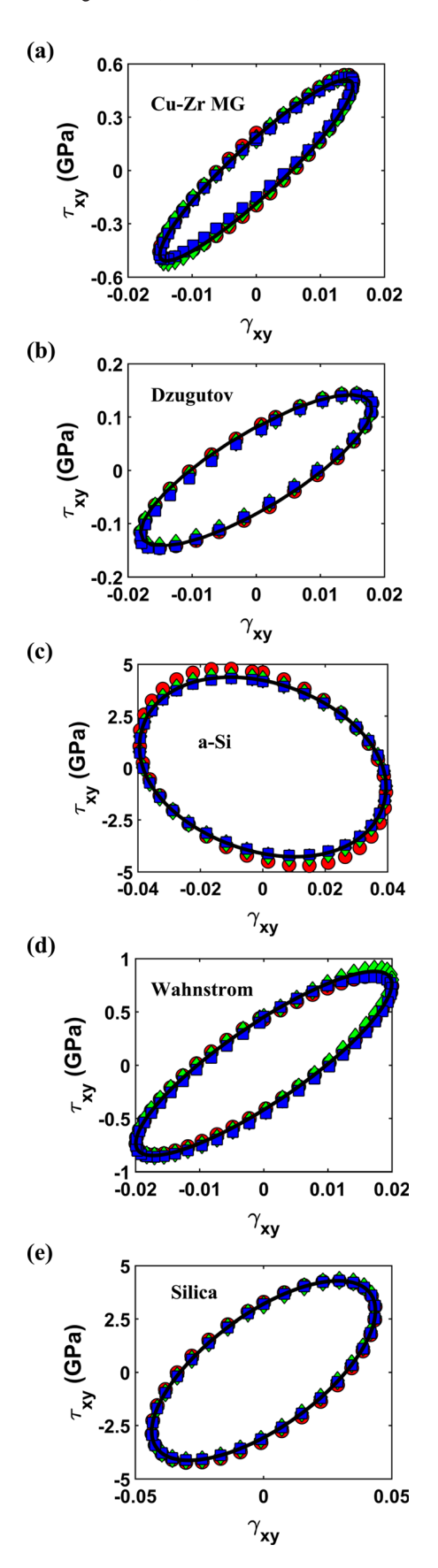


FIG. 7. Lissajous plots for stress-strain during oscillatory shear at the highest damping frequency (as shown in Fig. 6) for oscillatory shear deformation of all the glass models considered. The solid black line is the averaged data over 300 cycles. Data represented by colored markers correspond to stress-strain values from different cycle numbers, N (red  $(\bullet)$ ): N=5; green  $(\bullet)$ ): circle: N=50; blue  $(\blacksquare)$ : N=250).

the range of natural vibrational frequencies of the material is a direct consequence of large anharmonicity in the coupling between vibrational modes (phonons).<sup>25</sup> The predominant vibrational modes in glasses, denoted as "diffusons," lack a well-defined wave vector and polarization<sup>37</sup> as opposed to propagating, wavy, phonons in crystalline structures. An extensive body of work in dissipation in disordered solids points to the harmonic nature of damping, <sup>39,40,42</sup> where the vibrational eigenstates act as a system of act as damped harmonic oscillators. <sup>42,84</sup>

First, to check for correlation between the peak frequency for each glass (as obtained in Fig. 6) and the corresponding vibrational frequencies, we compute the vibrational density of states (DOS), g(f), from the Fourier transform of the velocity autocorrelation function. 85,86 Glasses show an excess in vibrational density of states (referred to as the Boson peak) in comparison to the Debye prediction.<sup>87</sup> The Boson peak is readily discerned as the peak in the reduced density of states,  $[g(f)/f^2]$ when plotted as a function of frequency. It is of immediate relevance to compare both the profiles of DOS, and the position of the Boson peak, with the frequency-dependence of damping. In Fig. 8, the loss moduli from Fig. 6 are plotted along with the DOS for all five glasses, with both sets of data normalized by their maximum for easy comparison of the frequency-dependence. Insets to the figure show the reduced density of states for each glass. Excess in the reduced DOS manifests as either as a broad peak or a bunch of peaks, with an additional divergent peak in the limit of zero frequency (the so-called quasi-elastic peak for frequencies below the range of interatomic potential<sup>88</sup>). It is immediately apparent that the loss moduli for glasses follow approximately the DOS (for network glasses, a-Si and silica, there are apparent differences in the profiles for frequency dependence of loss modulus and DOS that require a more detailed investigation). Additionally, an important observation is that the peak damping occurs at frequencies much larger than the Boson peak (typically an order of magnitude larger) for all glasses, consistent with a previous study on damping in a Lennard Jones glass.89

Another way to represent the relation between the peak damping frequency and the DOS is to look for correlations between the two. We plot the peak damping frequency as function of the weight-averaged vibrational frequency from the vibrational density of states (DOS),  $d_i$  in Fig. 9. The weight-averaged frequency was computed as  $f_{av} = \sum f_i.d_i/\sum d_i$  where,  $f_i$  is the DOS frequency. As seen from the figure, there exists a strong correlation between the two, signifying that damping in the THz regime essentially stems from the direct excitation of vibrational modes by the driving frequency. A detailed analysis of the excitation and discussion on the harmonic damping mechanism is presented in Sec. V.

## C. Damping in intermediate frequency—power-law scaling

At frequencies below the peak damping frequency, we observe that a distinct power-law scaling between the loss modulus and frequency exists. This can be observed clearly in Fig. 10, where loss moduli from Fig. 6 are plotted with a

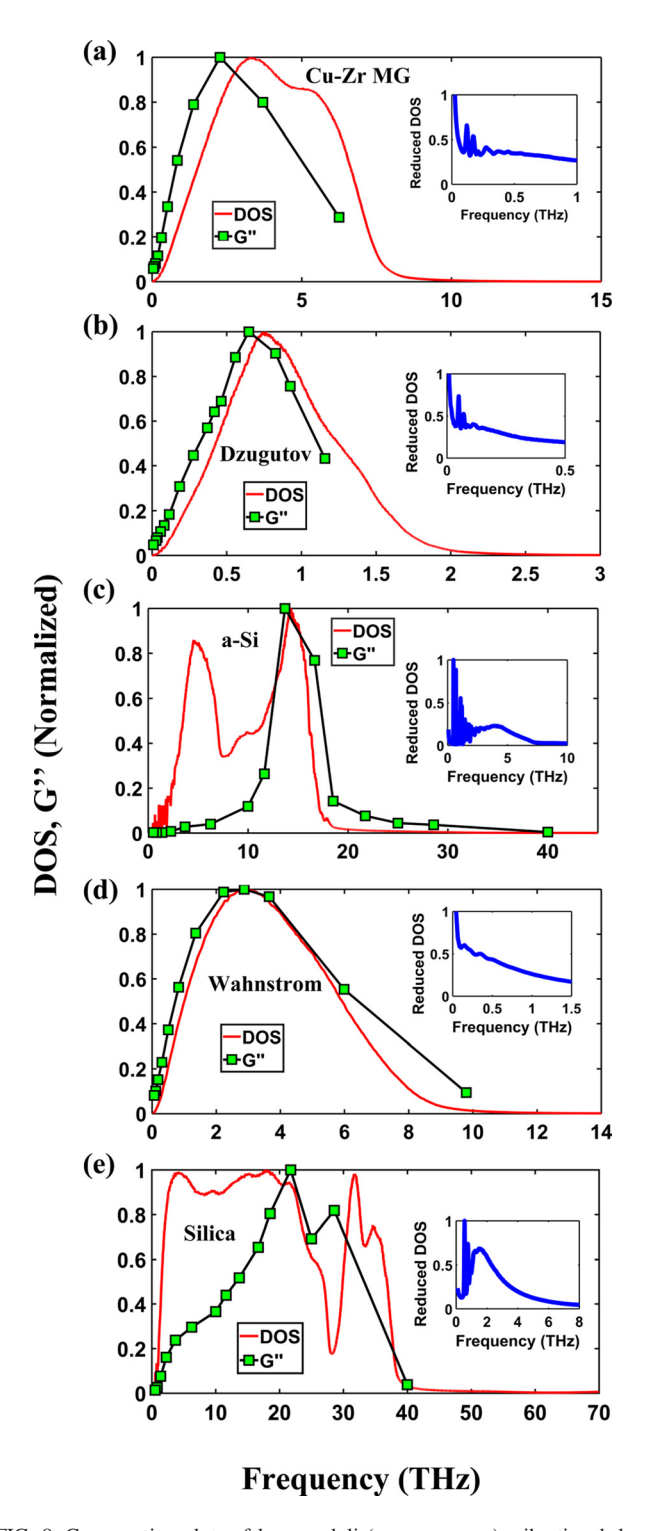


FIG. 8. Comparative plots of loss moduli (green squares), vibrational density of states (DOS) and reduced density of states (insets) for all five glasses. Loss moduli data are the same as those reported in Fig. 6.

log-log scale. The power-law exponents are noted for each glass. The scaling holds for intermediate frequencies for all glasses, down to  $\sim 50\,\mathrm{GHz}$  for the Cu-Zr MG, Dzugutov, and Wahnström glasses, and till  $\sim 100\,\mathrm{GHz}$  and  $\sim 1\,\mathrm{THz}$  for silica and a-Si. First, this scaling is consistent with a large body of work on sound attenuation  $^{90-93}$  and propagation of shock waves in viscoelastic materials  $^{94}$  and damping in nanomechanical resonators.  $^{33}$  They all exhibit a power-law scaling

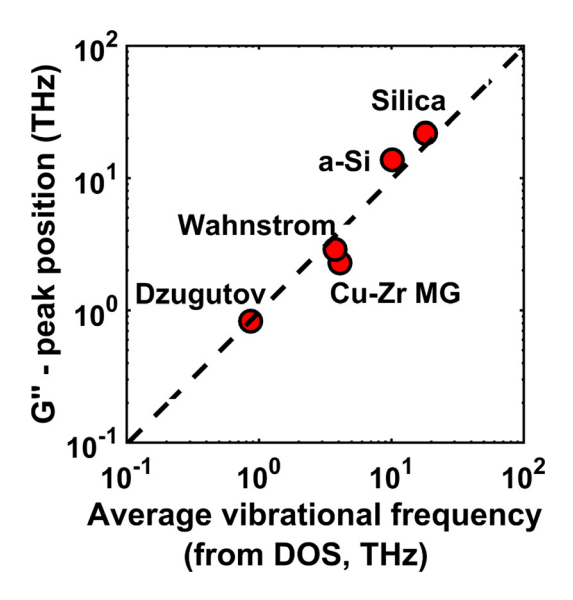


FIG. 9. Correlation between the peak position in the frequency-dependent loss modulus as obtained in Fig. 6 and the average frequency obtained from vibrational density of states (DOS) for each glass.

with respect to frequency, with a power law exponent ranging from 0 to 2.

Second, we note that the scaling for Cu-Zr MG, Dzugutov, and Wahnström glasses (which can be classified as "atomic" or "non-network" glasses) are all close to 1, and have a large goodness of fit. On the other hand, silica and a-Si (which are "network" glasses), show noticeable shoulders in the power-law fits, with a-Si showing a much larger exponent. We believe the nature of the power-law scaling in this frequency spectrum is inherently tied to the vibrational frequencies of the glass. As seen from the vibrational density of states plotted in Fig. 8, the noticeable peak positions for the acoustic and optical vibrational modes for silica and a-Si, approximately coincide with the shoulders observed in the loss moduli.

#### D. Low-frequency damping and structural relaxation

At frequencies below the power-law scaling regime, all glasses exhibit persistent damping, down to ~50 MHz (as seen in Fig. 6). With a view to explain this phenomenon, we take a cue from the inherent metastability of glasses that results in the formation of local deformation clusters, known as "soft spots," under loading. These soft spots are typically associated with shear transformation zones and eventual plastic deformation, <sup>62,64,95,96</sup> and could play a role in damping during the oscillatory shear deformation. Of particular importance would be the role of shear frequency employed on the evolution of such clusters. This mechanism is suppressed at frequencies corresponding to the high-frequency peak (in the THz range of vibrational frequencies) and leads to the persistent damping in the low-frequency regime. We note that in the low-frequency regime, averaging over a larger number of cycles was precluded by the high computational expense (see Fig. 6); however, loss modulus is expected to have acceptable stationarity, owing to the relatively slow rate of evolution of soft spots.

Here, we study the evolution of such soft spots or clusters as a function of shear frequency, for all the glasses and the

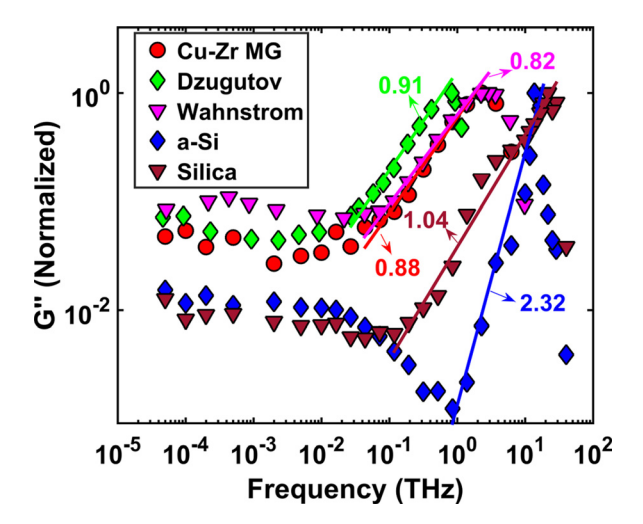


FIG. 10. Loss moduli data from Fig. 6 plotted in the log-log scale to demonstrate power-law variation near the high-frequency peak. Power-law exponents are indicated.

results are shown in Fig. 11. These simulations are performed under constant temperature (NVT) conditions, where the total time for shear deformation is fixed (as presented in Fig. 6). The total simulation time is fixed at 50 ns. The criterion for an atom to contribute to a cluster is that it should have a displacement at least equal to the shear amplitude and should

have at least one other displaced neighbor within a cutoff distance equal to the first shell of the nearest neighbors. This cutoff corresponds to the first minimum in the pair correlation function, g(r). We observed that a-Si and silica exhibited negligible cluster formation with this criterion, hence, the displacement amplitude was reduced to half the shear amplitude for these two cases.

Figure 11 shows the formation of both average cluster size and percentage of atoms that contribute to the clusters (the irreversibly deformed volume). For all glasses, we observe a decrease in cluster sizes for increasing frequency. Similarly, the volume of cluster atoms (panel b) shows a decreasing trend with increasing frequency. One exception here is the a-Si glass, which shows an increase in cluster volume (at 10 THz), albeit consisting of smaller cluster size compared to lower frequencies. This frequency-dependent cluster formation is, in fact, further accentuated for the case of constant number of shear cycles (as depicted in Fig. 6). We argue that the larger amount of time available for nucleation and growth of clusters at lower frequencies leads to a nearly-constant or even slightly increasing damping with decreasing frequency. A similar phenomenon for "viscous flow units" was observed by Wang et al. 97 during cyclic deformation of metallic glasses, albeit at high temperatures required for their activation, and by Priezjev<sup>98,99</sup> who demonstrated evolution of non-affine localized deformation during shear of a model binary Lennard-Jones glass.

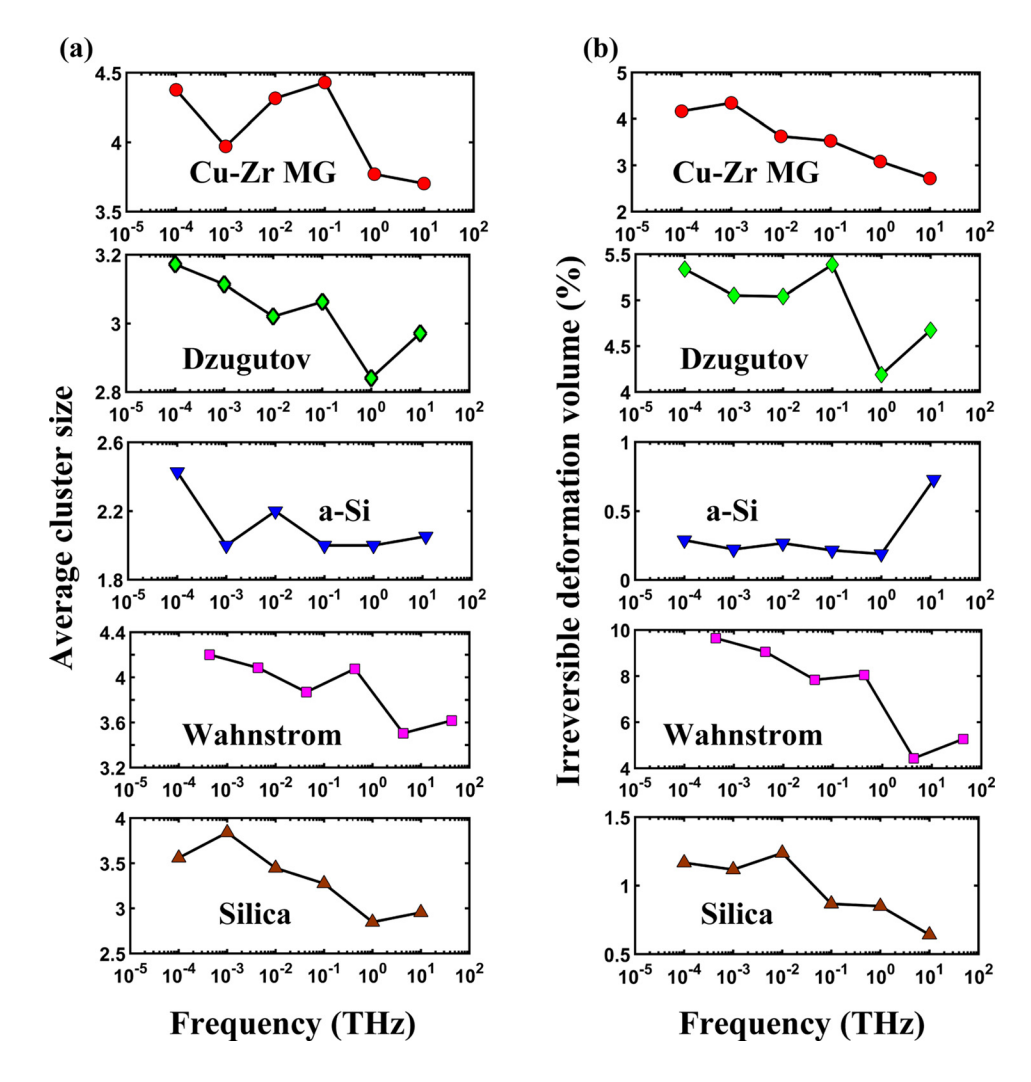


FIG. 11. Characterization of clusters ("soft spots") formed during constant-time oscillatory shear simulations for various glasses, as a function of shear frequency. The total simulation time at each frequency, for each glass is 50 ns. (a) Average cluster sizes at the end of 50 ns of oscillatory shear. (b) The total volume fraction of irreversibly deformed clusters at the end of shear. The general trend of increasing cluster size and volume with decreasing frequency is evident.

This low-frequency damping mechanism is a common feature in all glasses, but the extent of damping depends on the ease of formation of clusters, which in turn depends on the intermolecular forces at the atomic scale. We thus show that oscillatory shear deformation at low frequencies serve as a powerful probe for quantifying the ease of local atomic motion and the associated structural relaxation in glasses. On the other hand, at high frequencies approaching the THz regime (where cluster formation is suppressed), damping occurs *via* coupling between the harmonic vibrational eigenstates of the glass.

#### V. DISCUSSION

The harmonic nature of damping in disordered solids in the THz frequency, i.e., at frequencies corresponding to vibrational frequencies is well-established. In glasses, the Ioffe–Regel (IR) limit lefines the frequency at which the phonon mean free path becomes comparable with the wavelength. Above the IR limit, vibrational modes can no longer be defined with a wave-like character. Attenuation and damping in glasses, both below and above the IR limit have been shown to be harmonic in nature. Below this limit, elastic heterogeneities, i.e., heterogeneities in elastic moduli due to the inherent structural disorder act as scattering centers for propagation of vibrations, leading to harmonic Rayleigh scattering. Io2

Above the IR limit, and within the range of vibrational frequencies, Damart et al. 42 showed that damping arises from coupling between vibrational eigenmodes that act as damped harmonic oscillators. For a model silica glass, they showed that application of an oscillatory isostatic deformation gives rise to non-affine relaxations that in turn couple with the vibrational states. An alternate picture for harmonic energy dissipation in disordered, harmonic media can be found in the theory of thermal conductivity in disordered solids by Allen and Feldman. 103 They showed that, using a Kubo-Greenwood formalism, heat is transported by decoupled harmonic oscillators which are, in fact coupled by the temperature gradient. The delocalized vibrational eigenstates, resulting from superposition of the modes lead to non-zero off-diagonal elements of the density matrix. This translates to non-zero off-diagonal elements in the heat current operator, thus conducting heat. Thus, under non-equilibrium conditions, dissipation occurs due to direct coupling between harmonic modes in the presence of the non-equilibrium field (in this case, the oscillatory shear deformation).

A direct measure of the coupling between vibrational modes and the frequency of the input shear deformation is readily computed by measuring the temperature of each vibrational mode, T(f) during a non-equilibrium process (oscillatory shear in this case) according to Eq. (1), following the work of Shenogina *et al.*, <sup>104</sup>

$$T(f) = T_{EQ} \frac{\int_{f-\Delta f/2}^{f+\Delta f/2} C_{NE}(f') df'}{\int_{f-\Delta f/2}^{f+\Delta f/2} C_{EQ}(f') df'}.$$
 (1)

Here,  $C_{NE}$  and  $C_{EQ}$  are the velocity autocorrelation functions computed during the non-equilibrium (NE) shear process, and under equilibrium (EQ) respectively.  $T_{EO}$  is the system temperature in the absence of shear, i.e., under equilibrium. Numerical integration is performed over frequency windows of length  $\Delta f$ , centered at frequency f. Shown in Fig. 12 are the temperatures of vibrational modes calculated for Cu-Zr MG (panels a and b) and silica (panels c and d), during oscillatory shear at two frequencies close to the THz regime, and, which fall within the vibrational density of states for each glass. The equilibrium simulation was performed at 350 K ( $T_{EO} = 350$  K), and the corresponding shear simulations were performed over simulation times corresponding to a temperature rise from 300 K to 400 K, such that the average temperature equals  $T_{EO}$ . The only exception was for the silica simulation at  $f = 2.27 \,\text{THz}$ , where rapid and strong damping results in an average temperature  $\sim$ 580 K. Thus, the rise in temperature is modest in comparison to  $T_g$ . As can be clearly seen from the figure, the modes closest to the driving shear frequency (indicated by solid black lines) are selectively excited for all cases. This suggests that the energy pumped in via the plane wavelike shear deformation directly excites a set of vibrational modes whose frequencies overlap with the driving frequency, which subsequently dissipate energy harmonically. A signature for harmonic damping is its temperature-independence widely

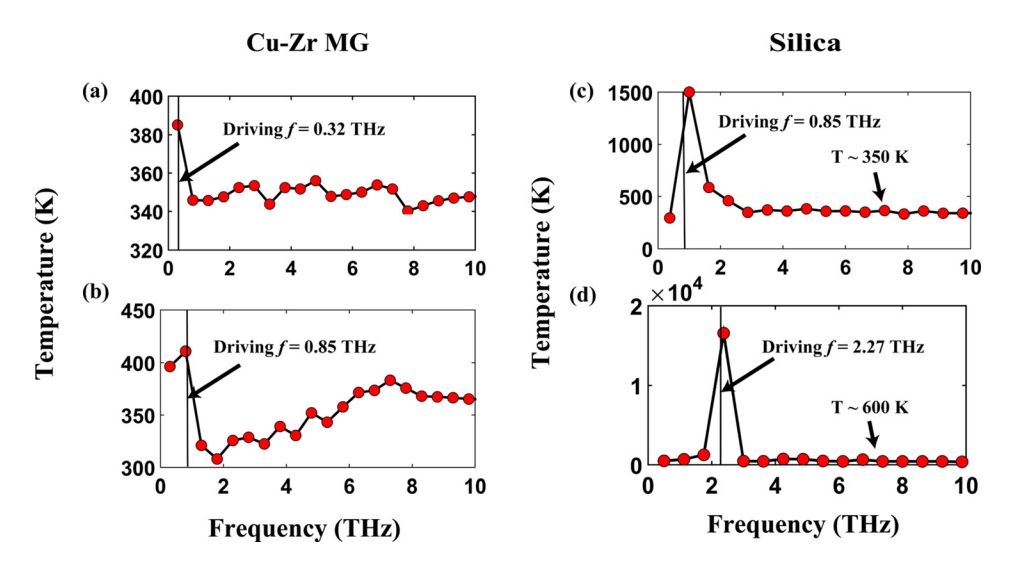


FIG. 12. Temperature of vibrational modes during shear at two frequencies, (a)  $f = 0.32 \,\text{THz}$  and (b)  $f = 0.85 \,\text{THz}$  for the Cu-Zr MG system, and at (c)  $f = 0.85 \,\text{THz}$  and (d)  $f = 2.27 \,\text{THz}$  for silica. The driving frequency is indicated by a solid line for each case. Temperatures of modes were calculated according to Eq. (1).

reported in literature,<sup>39–42</sup> which is also observed for the Cu-Zr MG system in this work (see Fig. 5), for silica (not shown here), and presumably for the other glasses considered in this work as well.

The above picture of excitation of vibrational frequencies holds only in the high-frequency regime; at frequencies far below the vibrational frequencies, the time scale associated with the shear period is much larger than the time for heat diffusion, and the predominant damping mechanism transitions to local plastic deformation (soft spots) as outlined in Sec. IVD. A large body of work in literature has dealt with studying the nature of local plastic events and shear transformations in amorphous solids under constant rate shear deformation; 105-107 it would be interesting to compare statistics of such cluster formation with the oscillatory shear case. Priezjev<sup>98,99</sup> studied the effect of periodic shear deformation on evolution of atomic rearrangements, and compared them with a no-shear, quiescent case. He showed that displacements are predominantly non-affine, the magnitude of which increases with strain amplitude. Interestingly, non-affine deformations were observed even for the quiescent case. In this context, we show that alternatively, lowering of shear frequency also leads to an increase in the cluster size (as seen in Fig. 11).

It is worthwhile to discuss our results for local atomic rearrangements (soft spots) in the context of  $\alpha$  and  $\beta$  relaxations in glass. Under oscillatory shear, these relaxations are characterized by the variation of loss modulus as a function of temperature, or equivalently, as a function of frequency as considered in this work.  $\alpha$  relaxation is associated with a peak in loss modulus close to  $T_g$ , while  $\beta$  relaxation is characterized by finite loss modulus at sub- $T_g$  temperatures (sometimes down to room temperature). 108–110 Alternatively,  $\alpha$  and  $\beta$  relaxations can be associated with low (< kHZ range) and high frequency (Hz to GHz regime) portions of the damping spectrum, depending on the properties of the glass, and the temperature.<sup>54</sup> Since we study damping of glasses at temperature close to 0.3  $T_g$ , and at frequencies spanning from MHz to THz, we rule out the role of  $\alpha$  relaxations completely. However, one cannot rule out the role of  $\beta$ relaxations in our results, considering the temperature at which the viscoelastic response is studied. Cohen et al. 110 used molecular dynamics to study the cooperative nature of beta relaxations in a model Lennard Jones glass under oscillatory shear, by pinning a small fraction of particles to the coordinate frame moving with the affine transformation describing the overall shear. Extending such a protocol to our glass models combined with novel experimental advancements may possibly reveal the role of beta relaxations in this frequency regime (~MHz). Broadband dielectric spectroscopic studies on structural glasses such as a-Si and silica may reveal additional insights on the frequency-dependence. Moreover, relaxation mechanisms in glasses, along with the associated atomic rearrangements depend strongly on the strain amplitude of the oscillatory shear. 111 Indeed, with respect to relaxation, the complex interplay between temperature, frequency, and strain amplitude for characterization of loss moduli may reveal further commonalities, and requires further detailed consideration.

Finally, an important control parameter during the shear simulations is the thermostat, and its role in the dissipation mechanism. We note that the role of thermostat in the high-frequency regime is negligible, as seen in Fig. 6 for shear in the presence and absence of a thermostat. Damart *et al.*<sup>42</sup> reported a qualitatively similar trend in the high-frequency damping for silica. However, at frequencies below the range of vibrational frequencies, they observed that the quality factor (or equivalently, the loss modulus) shows a direct scaling with the damping constant of the thermostat. This suggests that moduli in the intermediate and low frequencies reported here could be affected by the choice of the thermostat. However, qualitatively, damping in low frequencies arising *via* the local deformation of atomic clusters is expected to be present irrespective of the choice of the thermostat.

#### VI. SUMMARY AND CONCLUSIONS

Using non-equilibrium molecular dynamics oscillatory shear simulations, we have studied viscoelastic damping extensively in a model Cu-Zr metallic glass (MG), and show a striking commonality in damping characteristics for various glasses. The two important characteristics in the dependence of damping (as characterized by the loss modulus, G'') on shear frequency are: (a) the presence of a well-defined peak in the high-frequency (THz) regime and (b) persistent, nearlyconstant damping in the intermediate and low frequency regime. We show that the quench rate plays an important role in damping, especially at low frequencies—larger quench rates (glass at shallower energy minima) lead to a greater degree of local deformation, leading to larger damping. Closely associated with this is the time-dependent loss modulus for a glass with a large quench rate. The two other key factors are shear amplitude and shear temperature-shear amplitudes near and beyond the elastic limit exhibit nonlinear viscoelastic response and larger shear temperatures result in larger loss moduli in the low-frequency limit.

We show a clear correlation for the peak frequency (in the THz range) in damping response with the average vibrational frequency of glass. Vibrational modes close to the driving frequency are selectively excited, which then result in dissipation of energy harmonically. At intermediate and low frequencies (reaching down to ~50 MHz), we show that persistent damping in all glasses is a result of long time-scale local, irreversible deformation. From this study, we demonstrate that oscillatory shear deformation serves as a powerful probe for furthering mechanistic understanding of damping in the MHz to THz regime, and particularly in glasses, to quantify the degree of local atomic motion and associated stress relaxation at low frequencies.

#### **ACKNOWLEDGMENTS**

P.K. acknowledges support from the National Science Foundation (NSF) under Grant No. CMMI-1538730. Y.F.S. acknowledges support from the National Science Foundation (NSF) under Grant No. DMR-1207439. We are also grateful for the support from the Center for Computational Innovations (CCI) at the Rensselaer Polytechnic Institute. We thank Dr. David Rodney (University of Lyon) for helpful discussions.

- <sup>1</sup>A. K. Varshneya, Fundamentals of Inorganic Glasses (Elsevier, 2013).
- <sup>2</sup>W. Klement, R. H. Willens, and P. Duwez, Nature **187**, 869 (1960).
- <sup>3</sup>M. Telford, Mater. Today 7, 36 (2004).
- <sup>4</sup>M. F. Ashby and A. L. Greer, Scr. Mater. **54**, 321 (2006).
- <sup>5</sup>C. A. Schuh, T. C. Hufnagel, and U. Ramamurty, Acta Mater. **55**, 4067 (2007).
- <sup>6</sup>A. S. Argon, Acta Metall. **27**, 47 (1979).
- <sup>7</sup>A. Inoue, Acta Mater, 48, 279 (2000).
- <sup>8</sup>W. L. Johnson, J. Lu, and M. D. Demetriou, Intermetallics **10**, 1039 (2002).
- <sup>9</sup>J. Schroers and W. L. Johnson, Phys. Rev. Lett. **93**, 255506 (2004).
- <sup>10</sup>J. P. K. Doye, D. J. Wales, F. H. M. Zetterling, and M. Dzugutov, J. Chem. Phys. **118**, 2792 (2003).
- <sup>11</sup>Y. Q. Cheng, H. W. Sheng, and E. Ma, Phys. Rev. B 78, 14207 (2008).
- <sup>12</sup>E. Ma, Nat. Mater. **14**, 547 (2015).
- <sup>13</sup>D. B. Miracle, Nat. Mater. **3**, 697 (2004).
- <sup>14</sup>Y. O. Cheng and E. Ma, Prog. Mater. Sci. **56**, 379 (2011).
- <sup>15</sup>K. F. Yao and C. Q. Zhang, Appl. Phys. Lett. **90**, 061901 (2007).
- <sup>16</sup>H. Ma, J. Xu, and E. Ma, Appl. Phys. Lett. **83**, 2793 (2003).
- <sup>17</sup>A. Inoue, Mater. Trans. JIM **36**, 866 (1995).
- <sup>18</sup>C. J. Gilbert, R. O. Ritchie, and W. L. Johnson, Appl. Phys. Lett. **71**, 476 (1997).
- <sup>19</sup>L. S. Huo, J. F. Zeng, W. H. Wang, C. T. Liu, and Y. Yang, Acta Mater. 61, 4329 (2013).
- <sup>20</sup>W. Dmowski, T. Iwashita, C. P. Chuang, J. Almer, and T. Egami, Phys. Rev. Lett. **105**, 205502 (2010).
- <sup>21</sup>M. Hasegawa, S. Yamaura, H. Kato, K. Amiya, N. Nishiyama, and A. Inoue, J. Alloys Compd. 355, 37 (2003).
- <sup>22</sup>H.-R. Sinning, Phys. Rev. Lett. **85**, 3201 (2000).
- <sup>23</sup>T. Yagi, T. Imai, R. Tamura, and S. Takeuchi, Mater. Sci. Eng. A 370, 264 (2004).
- <sup>24</sup>N. Morito and T. Egami, Acta Metall. **32**, 603 (1984).
- <sup>25</sup>R. Ranganathan, R. Ozisik, and P. Keblinski, Composites, Part B **93**, 273
- <sup>26</sup>T. Lee, R. S. Lakes, and A. Lal, Rev. Sci. Instrum. **71**, 2855 (2000).
- <sup>27</sup>R. S. Lakes and J. Quackenbusch, Philos. Mag. Lett. **74**, 227 (1996).
- <sup>28</sup>K. Hyun, M. Wilhelm, C. O. Klein, K. S. Cho, J. G. Nam, K. H. Ahn, S. J. Lee, R. H. Ewoldt, and G. H. McKinley, Prog. Polym. Sci. 36, 1697 (2011)
- <sup>29</sup>J. C. Qiao and J. M. Pelletier, J. Mater. Sci. Technol. **30**, 523 (2014).
- <sup>30</sup>J. M. Pelletier, J. Alloys Compd. **393**, 223 (2005).
- <sup>31</sup>P. Wen, D. Q. Zhao, M. X. Pan, W. H. Wang, Y. P. Huang, and M. L. Guo, Appl. Phys. Lett. 84, 2790 (2004).
- <sup>32</sup>H. M. Wyss, K. Miyazaki, J. Mattsson, Z. Hu, D. R. Reichman, and D. A. Weitz, Phys. Rev. Lett. **98**, 238303 (2007).
- <sup>33</sup>Q. Unterreithmeier, T. Faust, and J. P. Kotthaus, Phys. Rev. Lett. 105, 027205 (2010).
- <sup>34</sup>R. Lifshitz and M. L. Roukes, *Phys. Rev. B* **61**, 5600 (2000).
- <sup>35</sup>X. Sun, K. Y. Fong, C. Xiong, W. H. P. Pernice, and H. X. Tang, Opt. Express 19, 22316 (2011).
- <sup>36</sup>C. Tomaras, B. Schmid, and W. Schirmacher, Phys. Rev. B 81, 104206 (2010).
- <sup>37</sup>J. Fabian and P. B. Allen, *Phys. Rev. Lett.* **82**, 1478 (1999).
- <sup>38</sup>H. R. Schober, J. Non-Cryst. Solids **357**, 501 (2011).
- <sup>39</sup>S. Taraskin and S. Elliott, Phys. Rev. B **61**, 12017 (2000).
- <sup>40</sup>G. Ruocco, F. Sette, R. D. Leonardo, G. Monaco, M. Sampoli, T. Scopigno, and G. Viliani, Phys. Rev. Lett. 84, 5788 (2000).
- <sup>41</sup>G. Baldi, V. M. Giordano, B. Ruta, R. Dal Maschio, A. Fontana, and G. Monaco, Phys. Rev. Lett. 112, 125502 (2013).
- <sup>42</sup>T. Damart, A. Tanguy, and D. Rodney, Phys. Rev. B **95**, 054203 (2017)
- <sup>43</sup>W. H. Wang, Prog. Mater. Sci. **57**, 487 (2012).
- <sup>44</sup>S. G. Ma, P. K. Liaw, M. C. Gao, J. W. Qiao, Z. H. Wang, and Y. Zhang, J. Alloys Compd. **604**, 331 (2014).
- <sup>45</sup>M. L. Lee, Y. Li, Y. P. Feng, and C. W. Carter, Intermetallics 10, 1061 (2002).
- <sup>46</sup>C. P. Chen and R. S. Lakes, J. Rheol. **33**, 1231 (1989).
- <sup>47</sup>T. Jaglinski, D. Kochmann, D. Stone, and R. S. Lakes, Science 315, 620 (2007).
- <sup>48</sup>G. Ruocco and F. Sette, J. Phys.: Condens. Matter **13**, 9141 (2001).
- <sup>49</sup>D. Heiman, D. S. Hamilton, and R. W. Hellwarth, Phys. Rev. B **19**, 6583 (1970)
- <sup>50</sup>J. Kieffer, Phys. Rev. B **50**, 17 (1994).
- <sup>51</sup>J. E. Masnik, J. Kieffer, and J. D. Bass, J. Chem. Phys. **103**, 9907 (1995).

- <sup>52</sup>P. H. Bolivar, M. Brucherseifer, J. G. Rivas, R. Gonzalo, I. Ederra, A. Reynolds, M. Holker, and P. de Maagt, IEEE Trans. Microwave Theory Tech. 51, 1062 (2003).
- <sup>53</sup>F. Kremer, J. Non-Cryst. Solids **305**, 1 (2002).
- <sup>54</sup>P. Lunkenheimer, U. Schneider, R. Brand, and A. Loid, Contemp. Phys. 41, 15 (2000).
- <sup>55</sup>P. Lunkenheimer and A. Loidl, Chem. Phys. **284**, 205 (2002).
- <sup>56</sup>P. Lunkenheimer, R. Wehn, T. Riegger, and A. Loidl, J. Non-Cryst. Solids 307–310, 336 (2002).
- <sup>57</sup>A. Alegría, J. Colmenero, K. L. Ngai, and C. M. Roland, Macromolecules 27, 4486 (1994).
- <sup>58</sup>F. Yuan and L. Huang, J. Non-Cryst. Solids **358**, 3481 (2012).
- <sup>59</sup>Y. Shi, J. Luo, F. Yuan, and L. Huang, J. Appl. Phys. **115**, 043528 (2014).
- <sup>60</sup>F. Delogu, Phys. Rev. B **79**, 184109 (2009).
- <sup>61</sup>Y. Shi and M. L. Falk, Acta Mater. **55**, 4317 (2007).
- <sup>62</sup>Z. D. Sha, S. X. Qu, Z. S. Liu, T. J. Wang, and H. Gao, Nano Lett. 15, 7010 (2015).
- <sup>63</sup>M. Zink, K. Samwer, W. L. Johnson, and S. G. Mayr, Phys. Rev. B 73, 172203 (2006).
- <sup>64</sup>F. Shimizu, S. Ogata, and J. Li, Mater. Trans. **48**, 2923 (2007).
- <sup>65</sup>S. Nose, J. Chem. Phys. **81**, 511 (1984).
- <sup>66</sup>W. G. Hoover, Phys. Rev. A **31**, 1695 (1985).
- <sup>67</sup>Y. Q. Cheng, E. Ma, and H. W. Sheng, Phys. Rev. Lett. **102**, 245501 (2009).
- <sup>68</sup>M. Dzugutov, Phys. Rev. A **46**, 2984 (1992).
- <sup>69</sup>J. Tersoff, Phys. Rev. B **39**, 5566 (1989).
- <sup>70</sup>G. Wahnström, Phys. Rev. A **44**, 3752 (1991).
- <sup>71</sup>B. W. H. van Beest, G. J. Kramer, and R. A. van Santen, Phys. Rev. Lett. 64, 1955 (1990).
- <sup>72</sup>F. Albano, N. Lacevic, M. L. Falk, and S. C. Glotzer, Mater. Sci. Eng. A 375, 671 (2004).
- <sup>73</sup>J. Tersoff, Phys. Rev. B **38**, 9902 (1988).
- <sup>74</sup>Y. Shi and M. L. Falk, Phys. Rev. B **73**, 214201 (2006).
- <sup>75</sup>M. E. Tuckerman, J. Alejandre, R. López-Rendón, A. L. Jochim, and G. J. Martyna, J. Phys. A: Math. Gen. 39, 5629 (2006).
- <sup>76</sup>M. Parrinello and A. Rahman, J. Appl. Phys. **52**, 7182 (1981).
- <sup>77</sup>G. J. Martyna, D. J. Tobias, and M. L. Klein, J. Chem. Phys. **101**, 4177 (1994).
- <sup>78</sup>W. Shinoda, M. Shiga, and M. Mikami, *Phys. Rev. B* **69**, 134103 (2004).
- <sup>79</sup>H. Sheng, J. He, and E. Ma, Phys. Rev. B **65**, 184203 (2002).
- <sup>80</sup>K. Vollmayr, W. Kob, and K. Binder, Phys. Rev. B **54**, 15808 (1996).
- <sup>81</sup>S. Munetoh, T. Motooka, K. Moriguchi, and A. Shintani, Comput. Mater. Sci. 39, 334 (2007).
- <sup>82</sup>L. Zhang, Y. Q. Cheng, A. J. Cao, J. Xu, and E. Ma, Acta Mater. 57, 1154 (2009).
- <sup>83</sup>S. Plimpton, J. Comput. Phys. **117**, 1 (1995).
- <sup>84</sup>P. Allen and J. Feldman, Phys. Rev. B **48**, 12581 (1993).
- <sup>85</sup>M. P. Allen and D. J. Tildesley, Computer Simulation of Liquids (Clarendon Press, 1987).
- <sup>86</sup>A. Rahman, J. Mandell, and J. P. McTague, J. Chem. Phys. **64**, 1564 (1976)
- <sup>87</sup>V. K. Malinovsky and A. P. Sokolov, Solid State Commun. 57, 757 (1986).
- 88 H. M. Flores-Ruiz, G. G. Naumis, and J. C. Phillips, Phys. Rev. B 82, 214201 (2010).
- <sup>89</sup>R. Ranganathan, Y. Shi, and P. Keblinski, Phys. Rev. B 95, 214112 (2017).
- 90T. L. Szabo, J. Acoust. Soc. Am. **96**, 491 (1994).
- <sup>91</sup>S. P. Näsholm and S. Holm, J. Acoust. Soc. Am. **130**, 3038 (2011).
- <sup>92</sup>T. Pritz, Appl. Acoust. **65**, 1027 (2004).
- <sup>93</sup>P. He, IEEE Trans. Ultrason. Ferroelectr. Freq. Control **45**, 114 (1998).
- <sup>94</sup>R. Rusovici, "Modeling of shock wave propagation and attenuation in viscoelastic structures," Ph.D. dissertation, 1999.
- <sup>95</sup>J. Ding, S. Patinet, M. L. Falk, Y. Cheng, and E. Ma, Proc. Natl. Acad. Sci. 111, 14052 (2014).
- <sup>96</sup>J. D. Ju, D. Jang, A. Nwankpa, and M. Atzmon, J. Appl. Phys. 109, 053522 (2011).
- <sup>97</sup>Z. Wang, P. Wen, L. S. Huo, H. Y. Bai, and W. H. Wang, Appl. Phys. Lett. 101, 121906 (2012).
- <sup>98</sup>N. V. Priezjev, Phys. Rev. E **94**, 23004 (2016).
- <sup>99</sup>N. V. Priezjev, Phys. Rev. E **93**, 13001 (2016).
- <sup>100</sup>S. Gelin, H. Tanaka, and A. Lemaître, Nat. Mater. **15**, 1177 (2016).
- <sup>101</sup>A. F. Ioffe and A. R. Regel, Prog. Semicond. **4**, 237 (1960).

- <sup>102</sup>H. Mizuno, S. Mossa, and J.-L. Barrat, EPL **104**, 56001 (2013).
- <sup>103</sup>B. Allen and J. L. Feldman, Phys. Rev. B **48**, 12581 (1993).
- <sup>104</sup>N. Shenogina, P. Keblinski, and S. Garde, J. Chem. Phys. **129**, 155105 (2008).
- <sup>105</sup>M. J. Demkowicz and A. S. Argon, Phys. Rev. Lett. **93**, 25505
- <sup>106</sup>M. J. Demkowicz and A. S. Argon, Phys. Rev. B **72**, 245205 (2005).
- <sup>107</sup>K. E. Jensen, D. A. Weitz, and F. Spaepen, Phys. Rev. E: Stat. Nonlinear, Soft Matter Phys. 90, 042305 (2014).
- <sup>108</sup>P. Rosner, K. Samwer, and P. Lunkenheimer, Europhys. Lett. **68**, 226 (2004).
- <sup>109</sup>H.-B. Yu and K. Samwer, Phys. Rev. B **90**, 144201 (2014).
- 110 Y. Cohen, S. Karmakar, I. Procaccia, and K. Samwer, Europhys. Lett. 100, 36003 (2012).
- P. Leishangthem, A. D. S. Parmar, and S. Sastry, Nat. Commun. 8, 14653
- (2016). <sup>112</sup>D. Wolf, P. Keblinski, S. R. Phillpot, and J. Eggebrecht, J. Chem. Phys. 110, 8254 (1999).
- <sup>113</sup>M. Elenius, T. Oppelstrup, and M. Dzugutov, J. Chem. Phys. **133**, 174502 (2010). 114S. Steeb and P. Lamparter, J. Non-Cryst. Solids **156**, 24 (1993).